Ab initio study of interacting lattice vibrations and stabilization of the β phase in Ni-Ti shape-memory alloy

Petros Souvatzis,[1] Dominik Legut,[2,3] Olle Eriksson,[2] and Mikhail I. Katsnelson[4]
[1]*Theoretical Division, Los Alamos National Laboratory, Los Alamos, New Mexico 87545, USA*
[2]*Department of Physics and Astronomy, Division of Materials Theory, Uppsala University, P.O. Box 530, SE-75121 Uppsala, Sweden*
[3]*Institute of Physics of Materials, Academy of Sciences of the Czech Republic, v.v.i., Žižkova 22, CZ-616 62 Brno, Czech Republic*
[4]*Institute for Molecules and Materials, Radboud University Nijmegen, NL-6525 ED Nijmegen, The Netherlands*
(Received 7 December 2009; revised manuscript received 30 January 2010; published 5 March 2010)

Lattice dynamical methods used to predict phase transformations in crystals typically evaluate the harmonic phonon spectra and therefore do not work in frequent and important situations where the crystal structure is unstable in the harmonic approximation, such as the β structure when it appears as a high-temperature phase of the shape memory alloy Ni-Ti. Here it is shown by self-consistent *ab initio* lattice dynamical calculations that the critical temperature for the premartensitic R-to-β phase transformation in Ni-Ti can be effectively calculated with good accuracy, and that the β phase is a result primarily of the stabilizing interaction between different lattice vibrations.

DOI: 10.1103/PhysRevB.81.092201 PACS number(s): 63.70.+h, 63.20.dk, 63.20.kg, 63.20.Ry

I. INTRODUCTION

Shape memory alloys (SMA) are compounds that after a mechanical deformation can, through heating, retain their original shape.[1] Due to their vast utilization in a broad spectrum of technologies, spanning areas such as medical applications to aerospace industry, there is an increased need for effective theoretical tools in the development and understanding of these alloys. Lately several theoretical studies have been made on one of the most commonly used SMA's, NiTi (nitinol), focusing on the martensitic transformation path[2,3] and on the shape-memory behavior.[4] Here the theoretical study of NiTi will be continued by applying the recently developed self-consistent *ab initio* lattice dynamical (SCAILD) method.[5]

The shape-memory effect in Ni-Ti is related to a reversible martensitic phase transformation into a monoclinic structure ($P2_1/m$, space group 11, Pearson symbol mP4) also known as B19′ phase[6] at around 273 K.[7–9] This phase transformation is preceded by a transformation at about 338 K from the austenite cubic phase (also known as the B2 or β phase, $Pm\bar{3}m$, space group 221, Pearson symbol cP2) into the R phase (P3, space group 143).[10] The mechanism behind the R-to-β transformation has been ascribed to the suppression of Fermi-surface nesting, resulting in a hardening of the T_2A phonon mode at the wave vector (and also nesting vector) $q=(\frac{1}{3},\frac{1}{3},0)$.[11]

Here, by means of first-principles calculations, an alternative picture of the mechanism behind this premartensitic phase transition will be provided. We will demonstrate that it is the interaction between different phonon modes that provides the main driving mechanism behind the stabilization of the β phase relative to the R phase in Ni-Ti. Since the β phase is dynamically unstable in the harmonic approximation over a large range of frequencies, not only at the wave vector $q=(\frac{1}{3},\frac{1}{3},0)$,[12,13] it is absolutely necessary to include anharmonic effects in any type of theoretical consideration when trying to understand the β-to-R phase transformation in Ni-Ti.

A straightforward calculation using first-principles molecular dynamics (MD) (Ref. 14) should, in principle, be able to reproduce the stability of the β phase for Ni-Ti, since MD implicitly include anharmonic effects. However, MD suffers from that it is a computationally very demanding task to obtain reliable free energies. Instead we will make use of the second-order nature of the displacive β-to-R phase transformation[10] and take the T_2A phonon mode displacement at the wave vector $\mathbf{q}=[\frac{1}{3}\frac{1}{3}0]$ as an order parameter. This will enable us to use the temperature dependence of the phonon mode in order to determine the critical temperature for phase transformation.

II. METHOD

In order to describe properly the phase transformation into the cubic phase for Ni-Ti one must include the interaction between phonons.[15] As a result, phonon frequencies turn out to be temperature dependent, which we explore numerically in this study by means of the SCAILD method.[5,16]

The SCAILD method is based on the calculation of Hellman-Feynman forces on atoms in a supercell. The method can be viewed as an extension of the frozen phonon method,[17] in which all phonons with wave vectors $\mathbf{q}$ commensurate with the supercell are excited together in the same cell by displacing atoms situated at the undistorted positions $\mathbf{R}+\mathbf{b}_\sigma$, according to $\mathbf{R}+\mathbf{b}_\sigma \rightarrow \mathbf{R}+\mathbf{b}_\sigma+\mathbf{U}_{\mathbf{R}\sigma}$, where the displacements are given by

$$\mathbf{U}_{\mathbf{R}\sigma}=\frac{1}{\sqrt{N}}\sum_{\mathbf{q},s}\mathcal{A}^{\sigma}_{\mathbf{q}s}\boldsymbol{\epsilon}^{\sigma}_{\mathbf{q}s}e^{i\mathbf{q}(\mathbf{R}+\mathbf{b}_\sigma)}. \quad (1)$$

Here $\mathbf{R}$ represents the N Bravais lattice sites of the supercell, $\mathbf{b}_\sigma$ the position of atom σ relative to this site, $\boldsymbol{\epsilon}^{\sigma}_{\mathbf{q}s}$ are the phonon eigenvectors corresponding to the phonon mode, s, and the mode amplitude $\mathcal{A}^{\sigma}_{\mathbf{q}s}$ is calculated from the different phonon frequencies $\omega_{\mathbf{q}s}$ through

$$\mathcal{A}^{\sigma}_{\mathbf{q}s} = \pm \sqrt{\frac{\hbar}{2M_{\sigma}\omega_{\mathbf{k}s}} \coth\left(\frac{\hbar\omega_{\mathbf{q}s}}{2k_B T}\right)}, \tag{2}$$

where T is the temperature of the system. Here the phonon frequencies

$$\omega_{\mathbf{q}s} = \left[-\sum_{\sigma} \frac{\epsilon^{\sigma}_{\mathbf{q}s} \cdot \mathbf{F}^{\sigma}_{\mathbf{q}}}{\mathcal{A}^{\sigma}_{\mathbf{q}s} M_{\sigma}} \right]^{1/2} \tag{3}$$

are obtained from the Fourier transform $\mathbf{F}^{\sigma}_{\mathbf{k}}$ of the forces acting on the atoms in the supercell.

Due to the simultaneous presence of all the commensurate phonons in the same force calculation, the interaction between different lattice vibrations is taken into account and the phonon frequencies given by Eq. (3) are thus renormalized by the very same interaction.

By alternating between calculating the forces on the displaced atoms and calculating new phonon frequencies and new displacements through Eqs. (1)–(3) the phonon frequencies are calculated in a self-consistent manner. For more details on the SCAILD method we refer to Refs. 5, 16, and 18.

It should be mentioned that we do not consider here the phonon-decay processes (see, e.g., Ref. 19 and references therein). Thus the question of how phonon linewidths obtained within the SCAILD framework are related to experimentally observed linewidths is still an open question. In the present calculations thermal-expansion effects have not been taken into account, and all calculations have been performed at the constant experimental lattice constant of 3.01 Å.[7,20]

As regards the computational details of the force calculation we used the VASP package,[21] within the generalized gradient approximation. The projector augmented wave potentials used required energy cutoffs of 300 eV. Methfessel-Paxton smearing of 0.2 eV was used together with a $8\times8\times8$ Monkhorst-Pack k-point grid. The supercell used was obtained by increasing the cubic primitive cell 3 times along the three primitive lattice vectors, resulting in a 54 atom supercell. Furthermore, the calculations were performed with $1\times3\times3$ supercells utilizing $45\times15\times15$ Monkhorst-Pack k-point grids, whereas the Fermi surfaces and general susceptibilities were calculated using a $100\times100\times100$ Monkhorst-Pack mesh.

III. RESULTS

Figure 1 shows the calculated phonon dispersions in cubic Ni-Ti for the temperatures 0, 200, 220, 240, 260, 280, and 300 K. The phonon-dispersion relation at $T=0$ K is very similar to the previous calculation done in Ref. 12, including imaginary frequencies along both directions (i.e., $[\xi,\xi,0]$ and $[\xi,\xi,\xi]$). The finite-temperature calculations predict the stability of the cubic phase of Ni-Ti by promoting the frequencies of the phonons along the Γ-to-R symmetry line and around the M symmetry point from imaginary to real for temperatures $\gtrsim$238 K.

Furthermore, the calculated $T=300$ K phonon dispersion is in good agreement with the experimental $T=400$ K data (black circles), with the exception of the lowest lying acoustic branch along the Γ-to-R symmetry line.

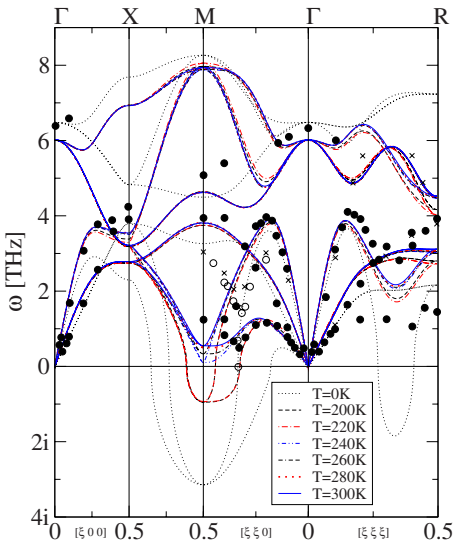

FIG. 1. (Color online) The phonon dispersions of β-NiTi calculated at different temperatures together with experimental data measured at 400 K (black circles), at 338 K (empty circles), and at 423 K (crosses) (Ref. 10). Solid, dashed, dotted, and dashed-dotted lines are the first-principles self-consistent phonon calculations.

Figure 2 shows the calculated squared T_2A phonon frequency at the wave vectors $q=(\frac{1}{2},\frac{1}{2},0)$ and $(\frac{1}{3},\frac{1}{3},0)$ at different temperatures together with experimental data. Here, as a result of a fourth-order anharmonic interaction, the expected linear dependence $\omega^2 \sim T$,[22] also suggested by experiment, is reproduced by the calculation.

The sudden jump in the calculated squared T_2A phonon frequencies at $T\sim227$ K (Fig. 2) can be related to the limited size of the supercell, since it overestimates the different phonon-mode contributions to the atomic displacements $\sim\frac{1}{\sqrt{N}\omega}$, especially in the temperature range where ω is close to zero. Thus by increasing the size of the supercell, i.e.,

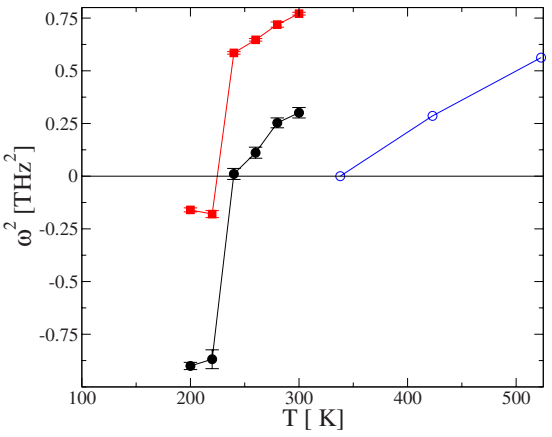

FIG. 2. (Color online) The calculated temperature dependence of the T_2A phonon frequency at $q=[\frac{1}{3}\frac{1}{3}0]$ (red squares) and at $q=[\frac{1}{2}\frac{1}{2}0]$ (black circles) in β-NiTi, here displayed together with experimental data for $q=(\frac{1}{3},\frac{1}{3},0)$ (empty blue circles) (Ref. 10). The width of the error bars are the square root of the mean-square deviation of the last 10 SCAILD iterations relative to the frequency of the 150th SCAILD iteration.

increasing the number of commensurate phonons, this overestimation can at least, in principle, be avoided. Furthermore, in the calculated phonon dispersion (Fig. 1) the dip or singularity in the T_2A phonon frequency is shifted from the experimental position $q=(\frac{1}{3},\frac{1}{3},0)$ to $q=(\frac{1}{2},\frac{1}{2},0)$. This shift originates from the singularity being confined to a relatively small region of q space, which also cannot be described adequately by a small supercell.[23] However, increasing the currently used $3\times3\times3$ supercell to the smallest larger cell accommodating the $q=(\frac{1}{3},\frac{1}{3},0)$ wave vector, would imply the use of a $6\times6\times6$ cell which was not pursued, due to computational reasons.

By using the phonon frequency of the T_2A mode at $q=(\frac{1}{3},\frac{1}{3},0)$ as an order parameter for the β-to-R phase transformation the critical temperature, T_c, corresponding to the transformation can be estimated to ~227 K. However, if instead the T_2A phonon frequency at $q=(\frac{1}{2},\frac{1}{2},0)$ is used as a order parameter we have $T_c\sim238$ K. This should be compared to the experimental value of 338 K. Since T_c depends strongly on the alloy composition (a change from 50 to 51 at. % Ni lowers T_c with up to 100 K) (Ref. 24) and on oxygen and carbon impurities,[25] the agreement must be viewed as good.

To investigate the relative importance between two of the possible processes involved in stabilizing the T_2A mode at $q=(\frac{1}{3},\frac{1}{3},0)$: (1) destruction of Fermi-surface nesting through the thermal smearing related to electronic excitations (used by Zhao and Harmon[11] to illustrate the effect of nesting suppression) or (2) phonon-phonon interactions, a series of additional first-principles electronic-structure calculations were performed. First, the frequency of the T_2A mode was calculated at different thermal smearings of the electronic subsystem, through a series of frozen phonon calculations.[17] The results of these calculations revealed that temperatures above 1000 K, i.e., much higher than the observed transition temperature, were required if thermal smearing was to be the only effect responsible for the stabilization of the T_2A phonon mode.

In the second step a series of Fermi-surface calculations were performed for the β-NiTi phase for different phonon-excited geometries. In Fig. 3(a) the Fermi surface of β-NiTi with no phonon-induced atomic disorder is shown. In Fig. 3(b) a cut, in the plane $k_z=0$, through the same Fermi surface as in Fig. 3(a) is shown, illustrating the nesting features. The Fermi Surface of the undistorted β structure was also calculated within a $3\times3\times3$ supercell, the result is displayed in Fig. 3(c). In Fig. 3(d) a cut through the Fermi surface is shown that has been calculated from four of the atomic configurations produced by the SCAILD scheme at $T=300$ K. This cut was taken through the surface $\langle E(\mathbf{k})\rangle=\langle E_F\rangle$, where $\langle E(\mathbf{k})\rangle$ and $\langle E_F\rangle$ are the arithmetical mean values of the Kohn-Sham eigenvalues, $E(\boldsymbol{k})$, and Fermi levels, E_F, calculated from the atomic configurations produced by the SCAILD scheme at $T=300$ K. Here $\mathbf{k}$ denotes a point in the space of k points.

Due to the down folding of the bands in Figs. 3(c) and 3(d), the nesting vector $q_n=(\frac{1}{3},\frac{1}{3},0)$ is shifted to $q=(0.177,0.177,0)$. Figures 3(c) and 3(d) show an apparent change in the Fermi-surface topology as the phonon-induced

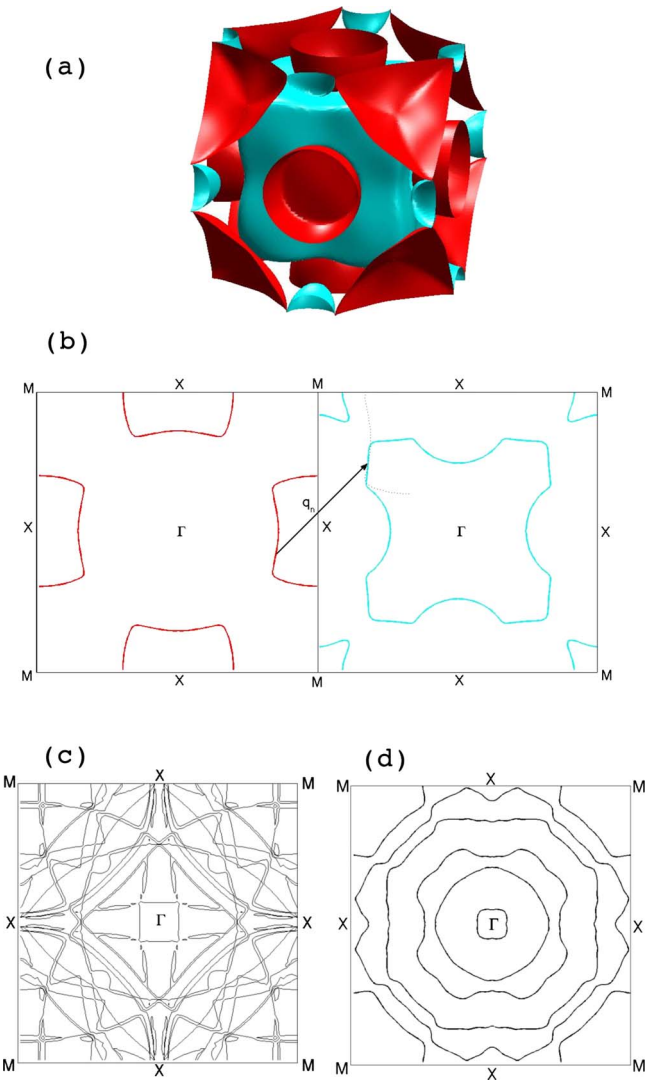

FIG. 3. (Color online) Fermi surface of the β-NiTi. In (a) the Fermi surface in the $T=0$ case (i.e., no phonon-induced disorder). In (b) we show the cut through the Fermi surface displayed in (a). The leftmost panel in (b) shows a cut through the red bowl-shaped surface sheets in (a). The rightmost panel in (b) shows a cut through the turquoise sheets in (a). In (b) the nesting vector $q_n=(\frac{1}{3},\frac{1}{3},0)$ interconnecting the nested parts of the Fermi surface is also shown. In (c) we show a cut through of the Fermi surface in (a) down folded to the first Brillouin zone of the undistorted $3\times3\times3$ super cell. In (d) we show a cut through the Fermi surface calculated from four of the $T=300$ K atomic configurations produced by the SCAILD scheme.

atomic disorder is introduced. However, to properly gauge the effect of atomic disorder upon the nesting features of β-NiTi, the susceptibility[23]

$$\chi(\mathbf{q})=\sum_{\mathbf{k}}\sum_{n,m}\frac{f[E_n(\mathbf{k}+\mathbf{q})]-f[E_m(\mathbf{k})]}{E_n(\mathbf{k}+\mathbf{q})-E_m(\mathbf{k})} \tag{4}$$

was also calculated for the same atomic configurations as was used in the Fermi-surface calculations. Here $f(E)$ is the Fermi-Dirac distribution function given by $f(E)$

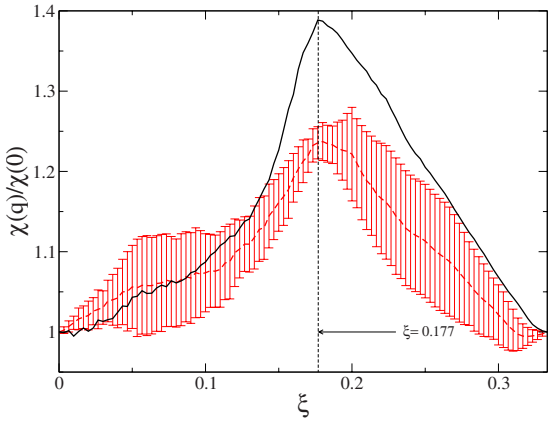

FIG. 4. (Color online) The calculated susceptibility as a function of $q=(\xi,\xi,0)$ in β-NiTi. The full black curve is the susceptibility for the $T=0$ K case (i.e., no phonon-induced disorder). The dashed red curve is the mean-susceptibility calculated from four of the $T=300$ K atomic configurations produced by the SCAILD scheme. Here the width of the error bars correspond to the standard deviation of the $T=300$ K susceptibility distribution. The susceptibilities are calculated within a $3\times3\times3$ supercell, resulting in a shift of the susceptibility peaks from $\xi=\frac{1}{3}$ to $\xi\approx0.177$, due to the down folding of the bands into the first Brillouin zone of the $3\times3\times3$ cell.

$=1/(e^{E-E_F/k_BT}+1)$. In Fig. 4 the results of these calculations are displayed, showing the suppression of the susceptibility peak as the phonon-induced atomic disorder is introduced. It should be noted that the suppression of the peak in $x(q)$ is quite pronounced. This demonstrates that the basic electronic structure of Ni-Ti is drastically different when the finite temperature excites collective lattice vibrations, compared to a $T=0$ calculation. Hence, it is this change in the electronic structure and the accompanying modification of the force-constant matrix, which is primarily responsible for the stabilization of the β phase. This explanation is hence somewhat more intricate and complex than the conventional model, of a smearing of a rigid electronic structure due to temperature effects of the Fermi-Dirac distribution function.

IV. CONCLUSION

To summarize, by first-principles SCAILD calculations, the cubic β phase in Ni-Ti has been shown to be stabilized by phonon-phonon interactions. Also, in the case of the unstable T_2A phonon mode at $q=(\frac{1}{3},\frac{1}{3},0)$ this interaction has been shown to be mediated through thermal-disorder-induced suppression of Fermi-surface nesting.

Furthermore, the SCAILD method has been proven an accurate and effective theoretical tool by predicting the critical temperature between $227\lesssim T_c\lesssim238$ K for the β-to-R premartensitic phase transformation, which is comparable with the experimental value of $T_c\sim338$ K.[10]

ACKNOWLEDGMENTS

The Department of Energy supported this work under Contract No. DE-AC52-06NA25396. We thank Bruce N. Harmon for all the helpful discussions.

[1] D. Shindo, Y. Murakami, and T. Ohba, Mater. Res. Bull. **27**, 121 (2002).
[2] N. Hatcher, O. Yu. Kontsevoi, and A. J. Freeman, Phys. Rev. B **79**, 020202(R) (2009).
[3] N. Hatcher, O. Yu. Kontsevoi, and A. J. Freeman, Phys. Rev. B **80**, 144203 (2009).
[4] X. Huang, G. J. Ackland, and K. M. Rabe, Nature Mater. **2**, 307 (2003).
[5] P. Souvatzis, O. Eriksson, M. I. Katsnelson, and S. P. Rudin, Phys. Rev. Lett. **100**, 095901 (2008).
[6] *Shape Memory Effects in Alloys*, edited by J. Perkins (Plenum, New York, 1975).
[7] K. Otsuka, T. Sawamutr, and K. Shimizu, Phys. Status Solidi A **5**, 457 (1971).
[8] D. Sandrock, A. J. Perkins, and R. F. Hehemann, Metall. Trans. **2**, 2769 (1971).
[9] V. G. Pushin, V. V. Komdrat'ev, and N. Khachin, Izv. Vyssh. Uchebn. Zaved. Fiz. **5**, 5 (1985) [Sov. Phys. J. **28**, 341 (1985)].
[10] H. Tietze, M. Müllner, and B. Renker, J. Phys. C **17**, L529 (1984); G. Herget, Ph.D. thesis, Johan Wolfgang Goethe Universitat, 1990.
[11] G. L. Zhao and B. N. Harmon, Phys. Rev. B **48**, 2031 (1993).
[12] K. Parlinski and M. Parlinska-Wojtan, Phys. Rev. B **66**, 064307 (2002).
[13] X. Huang, C. Bungaro, V. Godlevsky, and K. M. Rabe, Phys. Rev. B **65**, 014108 (2001).
[14] R. Car and M. Parrinello, Phys. Rev. Lett. **55**, 2471 (1985).
[15] M. I. Katsnelson, in *Encyclopedia of Condensed Matter Physics*, edited by G. F. Bassani, G. L. Liedl, and P. Wyder (Elsevier, Amsterdam, 2005), p. 77.
[16] P. Souvatzis, O. Eriksson, M. I. Katsnelson, and S. P. Rudin, Comput. Mater. Sci. **44**, 888 (2009).
[17] B. N. Harmon, W. Weber, and D. R. Hamann, Phys. Rev. B **25**, 1109 (1982).
[18] P. Souvatzis and S. P. Rudin, Phys. Rev. B **78**, 184304 (2008).
[19] M. I. Katsnelson, A. V. Trefilov, M. N. Khlopkin, and K. Yu. Khromov, Philos. Mag. B **81**, 1893 (2001).
[20] E. Goo and R. Sinclair, Acta Metall. **33**, 1717 (1985).
[21] G. Kresse and J. Furthmuller, Phys. Rev. B **54**, 11169 (1996).
[22] M. T. Dove, *Introduction to Lattice Dynamics* (Cambridge University Press, Cambridge, 2005); R. Blinc and B. Zeks, *Soft Modes in Ferroelectrics and Antiferroelectrics* (North-Holland, Amsterdam, 1974).
[23] M. I. Katsnelson, I. I. Naumov, and A. V. Trefilov, Phase Transitions **49**, 143 (1994).
[24] T. W Duerig and A. R. Pelton, *Materials Properties Handbook: Titanium Alloys* (ASM International, New York, 1994), pp. 1035–1048.
[25] E. Schüler, M. Bram, H. P. Buchkremer, and D. Stöver, Mater. Sci. Eng., A **378**, 165 (2004).